Revista de Metalurgia
July-September 2021, 57 (3), e201
ISSN-L: 0034-8570
https://doi.org/10.3989/revmetalm.201

Wear behavior and corrosion properties of Age-hardened AA2010 aluminum alloy

Nilay Çömez*

Manisa Celal Bayar University, Metallurgical and Materials Engineering Department, Manisa, Turkey

(*Corresponding author: nilay.comez@cbu.edu.tr)

Submitted: 27 November 2020; Accepted: 22 June 2021; Available On-line: 23 September 2021

ABSTRACT: This study aims to investigate the wear and corrosion resistance after heat treatment of AA2010 alloy. AA2010 alloy was solutionized at 500 °C for 1 h, and then quenched in water at room temperature. Solution treatment was followed by aging treatment at 160 °C for 16, 18, and 22 h. Peak hardness was achieved at 18 h. Ball-on-disc wear test caused cold deformation and hence increased the hardness of the worn surface locally. The corrosion rate of heat treated AA2010 alloy was determined according to Tafel extrapolation method. Corrosion test was carried out in 3.5 wt.% NaCl solution at room temperature. The minimum corrosion rate was obtained in 18 h aged AA2010 alloy. For moderate wear resistance and good corrosion resistance, 18 h aging is recommended for AA2010 alloy. Both the intergranular and pitting corrosion mechanisms were observed on the corroded surface of the AA2010 alloy.

KEYWORDS: Aging; Aluminum; Corrosion; Hardness; Tafel; Wear

Citation/Citar como: Çömez, N. (2021). "Wear behavior and corrosion properties of Age-hardened AA2010 aluminum alloy". *Rev. Metal.* 57(3): e201. https://doi.org/10.3989/revmetalm.201

RESUMEN: *Comportamiento al desgaste y propiedades de corrosión de la aleación de aluminio AA2010 endurecida por envejecimiento*. El presente estudio tiene como objetivo investigar la resistencia al desgaste y las propiedades de corrosión de la aleación AA2010 tratada térmicamente. La aleación se disolvió a 500 ºC durante 1 h y luego se inactivó en agua a temperatura ambiente. El tratamiento en solución fue seguido por un tratamiento de envejecimiento a 160 °C durante 16, 18 y 22 h. La dureza máxima se alcanzó a las 18 h. La prueba de desgaste utilizando un disco de bola provocó una deformación en frío y, por tanto, aumentó localmente la dureza de la superficie desgastada. La velocidad de corrosión de la aleación AA2010 tratada térmicamente se determinó mediante el método de extrapolación de Tafel. Los ensayos de corrosión se llevaron a cabo en NaCl al 3,5% a temperatura ambiente. La velocidad mínima de corrosión se obtuvo con la aleación envejecida 18 h. Así, para una resistencia moderada al desgaste y buenas propiedades frente a la corrosión, se recomienda un envejecimiento de 18 h. Finalmente, se observó corrosión intergranular y corrosión por picadura en la superficie de la aleación.

PALABRAS CLAVE: Aluminio; Corrosión; Desgaste; Dureza; Envejecimiento; Tafel

ORCID ID: Nilay Çömez (https://orcid.org/0000-0002-6432-6582)

1. INTRODUCTION

Weight reduction of vehicles is one of the most focused problems in the automotive industry for fuel saving. Aluminum alloys are remarkable materials that can overcome the weight obstacle of automobiles due to their low density. In addition, they exhibit good deformability and machinability, high strength-weight ratio and corrosion resistance (Sadeler *et al.*, 2004; Sun *et al.*, 2013). In particular, heat treatable aluminum alloys can provide many profits by a suitable aging process. For this reason, artificial aging of aluminum alloys is studied by many researchers. For instance, Taştan *et al.* (2019) applied artificial aging process to AA6082 and AA7075 alloys by conventional heating and induction heating. Similarly, Çavdar *et al.* (2021) achieved artificial aging of AA5083 and AA2024 by induction heating procedure.

2xxx series belongs to the heat treatable aluminum alloy class and is employed in particular, in aerospace and automotive industry (Tariq *et al.*, 2012). 2xxx series alloys need copper as an alloying element to be able to harden by precipitation. Hardness is accepted as the main criteria for the consideration of wear behavior of materials. It is well-known that construction equipment becomes useless because of wear (Meyveci *et al.*, 2010). Hardness of 2xxx series alloys can be increased by precipitation hardening resulting in an ordered precipitate structure. Hence, the wear resistance is expected to be improved (Meyveci *et al.*, 2010; Tariq *et al.*, 2012). Although the intermetallic compounds of copper such as Al_2Cu and Al_2CuMg improve the strength by precipitation hardening, they increase the susceptibility of localized corrosion (pitting) and oxidation of 2xxx series, in particular, in an aqueous medium containing chloride ions (Staley, 2016; Arunachalam *et al.*, 2018; Totten *et al.*, 2018).

Corrosion behavior of AA2024 was studied by several researchers. Menan and Henaff (2009) investigated the corrosion fatigue crack growth behavior of AA2024. Liao *et al.* (1998) observed the pitting corrosion in AA2024 by in-situ monitoring. A similar study was carried out by Kang *et al.* (2010). They revealed the pitting corrosion behavior of friction stir welded joint of AA2024-T3 by in-situ observation technique. In addition, Mishra and Balasubramaniam (2007) investigated the effect of $LaCl_3$ and $CeCl_3$ chlorides on the corrosion inhibition of AA2014 alloy. However, they did not consider the heat treatment condition of AA2014. Apart from the corrosion of 2xxx series aluminum alloys, wear behavior of these alloys, in particular AA2024, was studied by Kaçar *et al.* (2003), Meyveci *et al.* (2009), Abarghouie and Reihani (2010), and Kaczmar and Naplocha (2010).

AA2010 alloy can be used as structural sheet material in vehicle body (e.g., inner and outer hood panels of Lincoln Towncar) (Hussey and Wilson, 1998; Totten *et al.*, 2018). There is no study in the literature about corrosion and wear behaviors of AA2010 aluminum alloy. This study aimed to investigate the corrosion resistance and wear characteristic of AA2010 alloy after precipitation hardening process. The effect of aging time on corrosion and wear behavior of AA2010 alloy was discussed.

2. MATERIALS AND METHODS

2.1. Sample Preparation and heat treatment process

Before the aging process, samples were cut and prepared for microstructural investigations, hardness, wear, and corrosion tests. The spectral analysis of AA2010 alloy is given in Table 1. AA2010 alloy was solution treated at 500 °C for 1 hour and aged at 160 °C for 16, 18, and 22 hours. Polished samples were etched with aqueous NaOH solution (10 g NaOH+50 ml distilled water) and examined under an optical microscope.

2.2. Hardness and Wear Tests

Macro hardness of the heat treated samples was measured by Vickers indenter under 2 kg-force loads. In addition, the micro Vickers hardness test was applied on the worn surface under 300 g-force loads.

Wear test of heat treated samples was carried out with CSM instruments (Fig. 1), ball-on-disc wear-test apparatus under 2 N loads at room temperature. Alumina ball with a diameter of 6 mm was used as a counterpart. Each test was performed with a constant sliding speed of 5 cm/s and the track radius was 2.5 mm. Wear loss was measured every 100 m distance with the aid of a Mitutoyo profilometer. Total sliding distance of the wear test was 500 m.

2.3. Corrosion test

Corrosion test was conducted by linear polarization resistance method using Metrohm DropSens Potentiostat (Fig. 2). The corrosion rate of heat treated AA2010 alloy was determined by Tafel curves. 30 mm^2 area of each sample was immersed

Table 1. Chemical composition of AA2010 (wt.%)

Cu	Zn	Mg	Si	Fe	Mn	Cr	Al	Other
0.87	0.83	0.779	0.461	0.444	0.255	0.068	96.19	0.099

Figure 1. CSM instruments ball-on-disc wear test apparatus.

in 100 ml 3.5 wt.% sodium chloride (NaCl) solution for corrosion test. The three-electrode corrosion cell system is composed of the AA2010 sample as a working electrode, Ag/AgCl electrode as a reference electrode and a graphite electrode.

Before starting the test, open circuit potential (OCP) was measured for 60 seconds. Then Tafel curves from a cathodic potential of -0.8 V to an anodic potential of 1 V were plotted. All measurements were carried out with the scanning rate of 0.001 V/s.

3. RESULTS AND DISCUSSION

3.1. Corrosion and microstructure

The microstructure image of AA2010 alloy is given in Fig. 3a. Micro-scaled Al-Fe intermetallic particles were observed by SEM-EDX (Fig. 3b). According to Al-Fe phase diagram (Baker, 1992), the given composition indicates the formation of FeAl and/or Fe_3Al intermetallic particles. This prediction was proved by the XRD analysis. A peak of Fe-Al intermetallic phase was detected by XRD. In addition, the main precipitation hardening phases of 2XXX

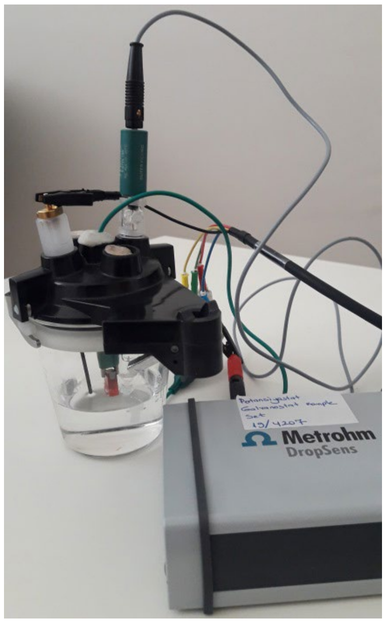

Figure 2. Corrosion test equipment.

series aluminum alloy such as Al_2Cu and Al_2CuMg were observed (Fig. 4). The intensity of the peaks of Mg_2Si and $MgZn_2$ precipitation hardening phases was found to be less than Al_2Cu and Al_2CuMg. Hence, the determinant factor of corrosion in terms of microstructure is thought to be the change of size and distribution of Al_2Cu and Al_2CuMg as discussed in the following paragraphs.

Open-circuit potential (OCP) graphic indicates the tendency of dissolution of 22 h aged sample with a more negative OCP (approximately -0.76 V). 16 h and 18 h aged samples have approximately -0.71 V OCP, hence less tendency of corrosion is expected for these samples (Fig. 5).

Tafel curves of AA2010 alloy, aged for 16, 18 and 22 hours are given in Fig. 6. Jcorr (current density) and Ecorr (corrosion potential) are given in Table 2. Ecorr is almost same for all samples (Fig. 6 and Table 2). The corrosion rate directly depends on the

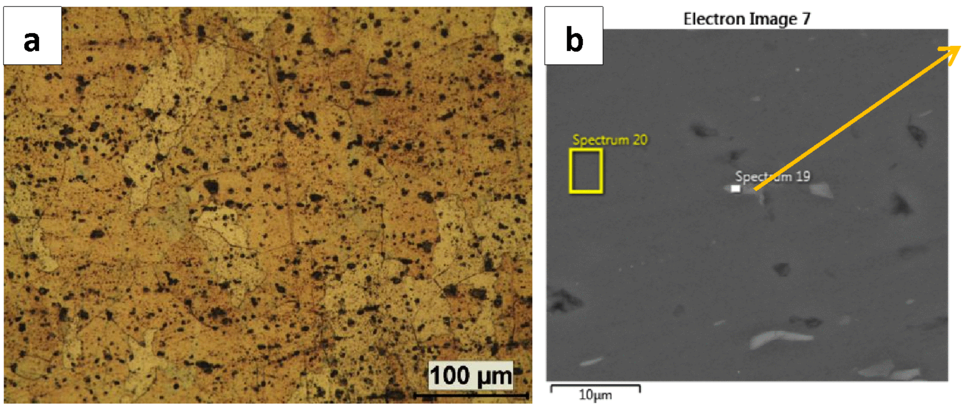

Element	wt.%
Al	76.55
Fe	12.70
Si	4.92
Cu	2.34
Mn	2.18
Cr	0.44
Zn	0.43
Mg	0.43
Total	100.00

Figure 3. a) Optical microscope image of AA2010 alloy, and b) SEM-EDX analysis of the intermetallic particle.

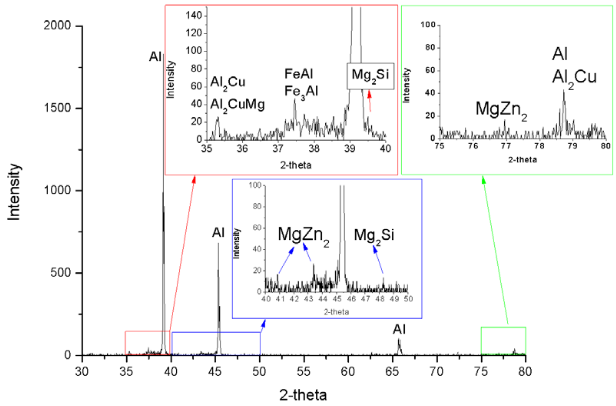

Figure 4. XRD graphic of 18 h aged sample.

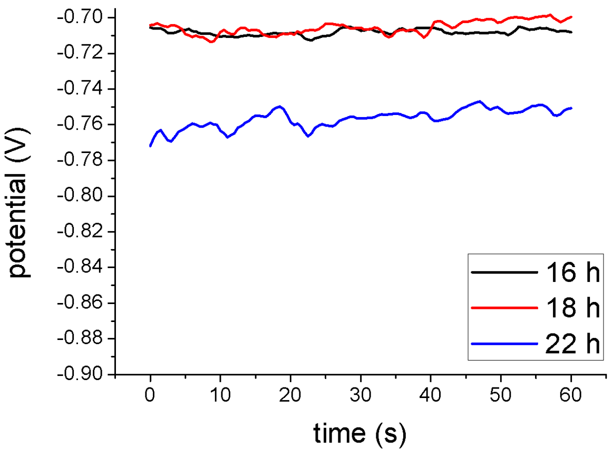

Figure 5. Open-circuit potential graphics.

Table 2. E_{corr}, J_{corr}, and corrosion rate values of aged AA2010 alloy in 3.5 wt.% NaCl solution obtained by Tafel extrapolation method

Aging hour	E_{corr} (V)	J_{corr} (μA·cm^{-2})	Corrosion rate (mm/year)
16	-0.67	3.78	0.041
18	-0.68	3.58	0.039
22	-0.71	5.12	0.056

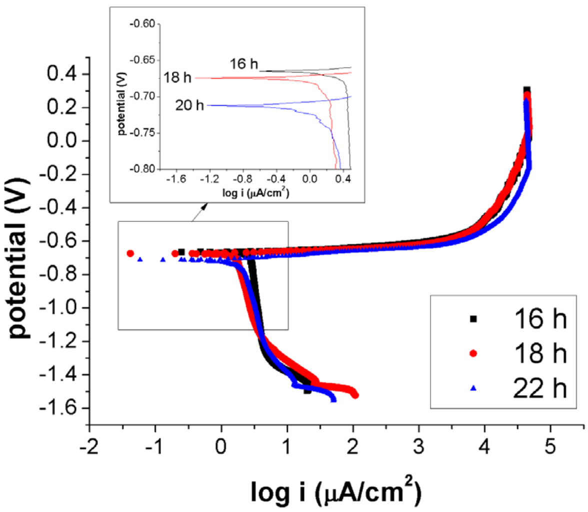

Figure 6. Tafel curves of aged samples for 16, 18, and 22 h.

current density (Jcorr) corresponding to the intersection point of the anodic and cathodic slopes of the Tafel curve (Bilgiç, 2018). Both the current density and corrosion rate of 16 h and 18 h aged samples are approximately equal to each other. However, increasing the aging time further increased the corrosion current and accordingly corrosion rate.

Optical microscope images of corroded surfaces clearly indicate the formation of intergranular corrosion and pitting corrosion (Fig. 7). The pitting corrosion occurs due to the galvanic coupling of the cathodic intermetallic particles and anodic aluminum matrix. Al-Fe intermetallic particles arise from the interaction between alloying elements and impurities during the casting process. They are not affected by solution heat treatment or aging (Andreatta *et al.*, 2004). However, intermetallic particles have a significant effect on corrosion. They cause discontinuities in the surface film formed in aqueous solution and promote the local breakdown of the passive oxide film. Once the oxide layer is damaged, dissolution of the aluminum matrix accelerates (Chen *et al.*, 1996; Mishra and Balasubramaniam, 2007; Krishna *et al.*, 2017). Micro scaled Al-Fe intermetallic particles (Fig. 3b) worked as a cathode resulting in anodic dissolution of aluminum matrix (Yasakau *et al.*, 2007), hence they caused pitting corrosion of AA2010 samples independently of aging time (Fig. 7 and Fig. 8). Apart from the Al-Fe intermetallic particles, 2XXX series aluminum alloys include strengthening Al_2Cu, and Al_2CuMg precipitations (Wang and Starink, 2005; Burt, 2015) as detected by XRD analysis in the present study. Here, Al2Cu phase takes place as cathode side in galvanic coupling of aluminum matrix and precipitate, hence accelerates the oxidation of aluminum and formation of corrosion pits (Burt, 2015; Vieira *et al.*, 2011). However, Al_2CuMg tends to precipitate along the grain boundary and generates a copper depleted zone. Both Al_2CuMg phase and copper depleted zone along the boundaries exhibit anodic characteristic in comparison with the surrounding matrix (Burt, 2015). Consequently, it was thought that intergranular corrosion was promoted

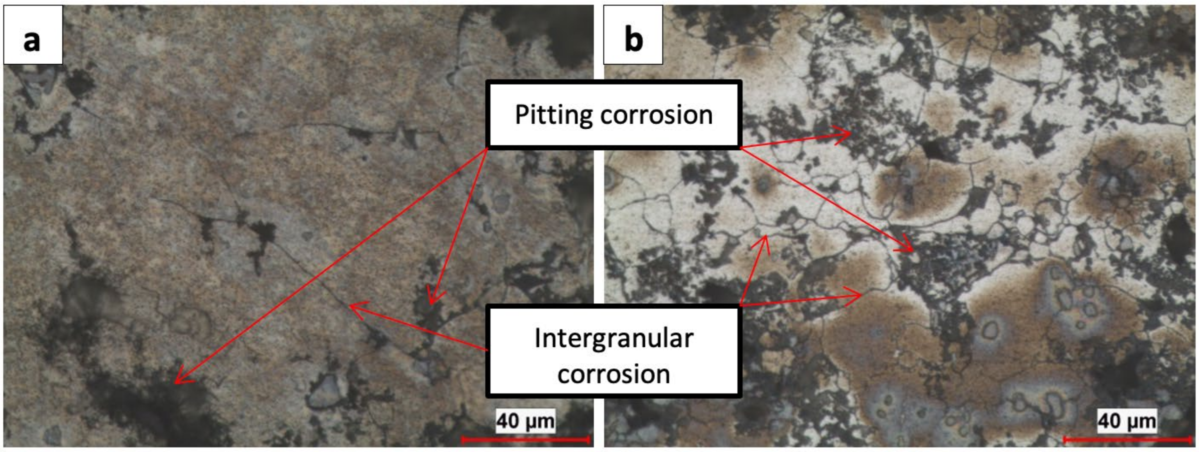

Figure 7. Optical microscope images of corroded surfaces: a) 18 h, b) 22 h.

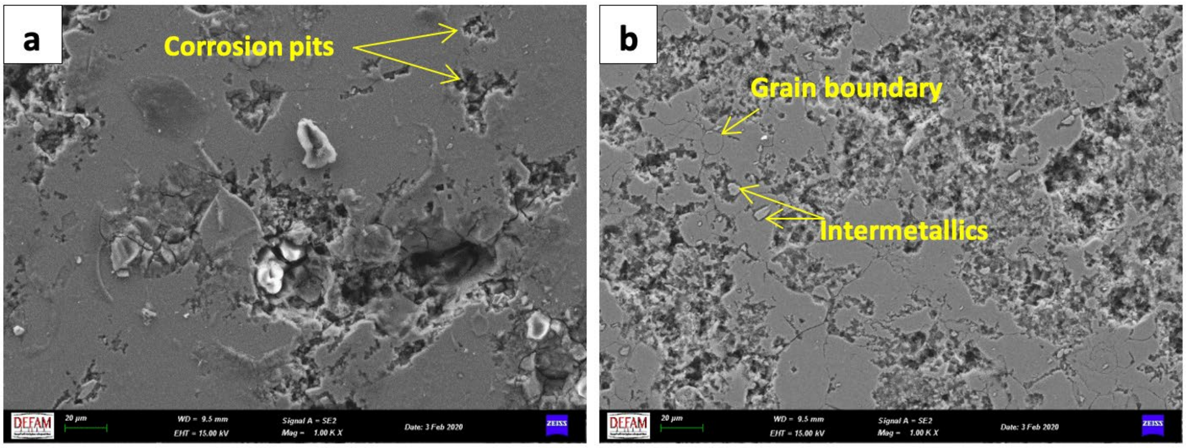

Figure 8. SEM images of corroded surfaces: a) 18 h, b) 22 h.

in the overaged sample by the coarsened Al_2CuMg precipitations and generated copper depleted zone. In addition, anodic precipitates within the grain boundary such as Mg_2Si and $MgZn_2$ (Gharavi *et al.*, 2015; Liu *et al.*, 2016) that were detected by XRD promote the intergranular corrosion. The overaged sample which was aged for 22 h showed maximum corrosion rate owing to the total effect of pitting and intergranular corrosion. Both the pitting and intergranular corrosions are the dominant corrosion mechanisms for overaged sample, whereas 18 h aged sample mainly suffered from pitting corrosion (Fig. 7). Even so, pitting corrosion damaged the overaged sample more than 18 h aged one as it is seen in SEM images (Fig. 8).

In summary, 22 h aged sample exhibits the maximum corrosion rate of 0.056 mm/year as predicted from OCP value, whereas 18 h aged sample with the peak strength exhibits a minimum corrosion rate of 0.039 mm/year (Table 2). Because, reaching the peak strength by artificial aging significantly reduces the intergranular corrosion susceptibility. Artificial aging up to peak strength avoids the development of the copper depleted zone by eliminating the precipitation of coarse Al_2CuMg phase along the grain boundary. As a consequence, intergranular corrosion can be got under control (Burt, 2015; Krishna *et al.*, 2017).

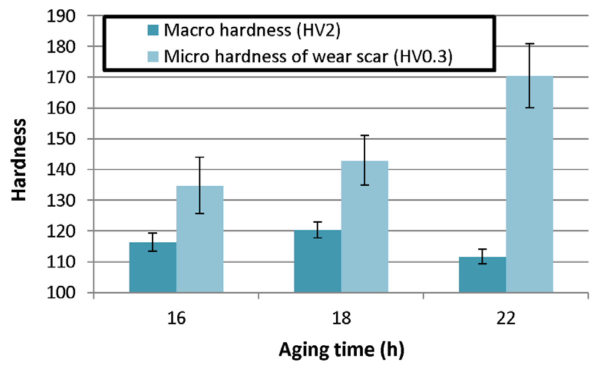

Figure 9. Relation between aging time and hardness before and after the wear test.

3.2. Hardness and wear tests

The average macro hardness of the as-received AA2010 alloy is 85.27 HV. Macro hardness values of heat treated AA2010 alloy are given in Fig. 9.

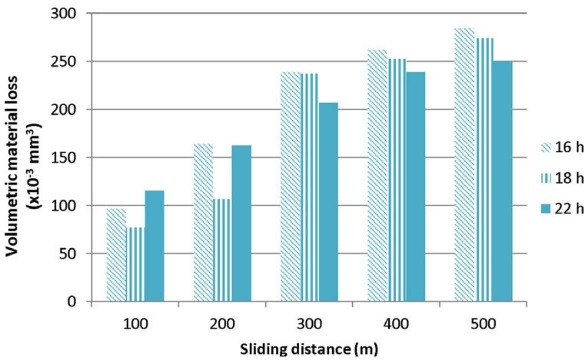

Figure 10. Volumetric material loss.

Peak hardness was obtained after 18 h aging process and was found to be 120 HV on the average. 22 h aging process caused over aging and the hardness decreased to 111 HV. As it was noticed in the study of Meyveci *et al.* (2012), prolonged aging time resulted in a decrease in hardness of heat treatable aluminum alloys due to the over aging phenomenon. The artificial aging heat treatment increased the hardness of AA2010 alloy by 30% - 40%.

Volumetric material loss-sliding distance graphic of aged samples are given in Fig. 10. Meyveci *et al.* (2011) reported that the wear loss depends on aging temperature and aging time. Up to 200 meters, minimum wear loss was observed in 18 h aged sample

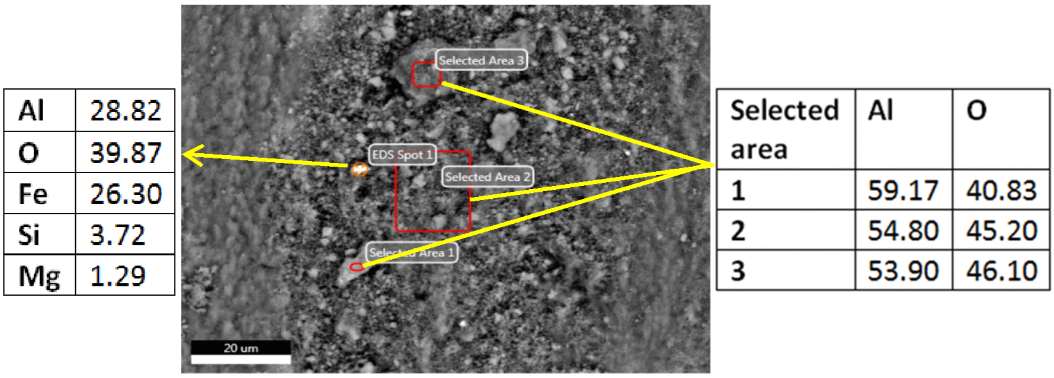

Figure 11. SEM-EDX analysis from the worn surface of 22 h aged specimen (wt.%).

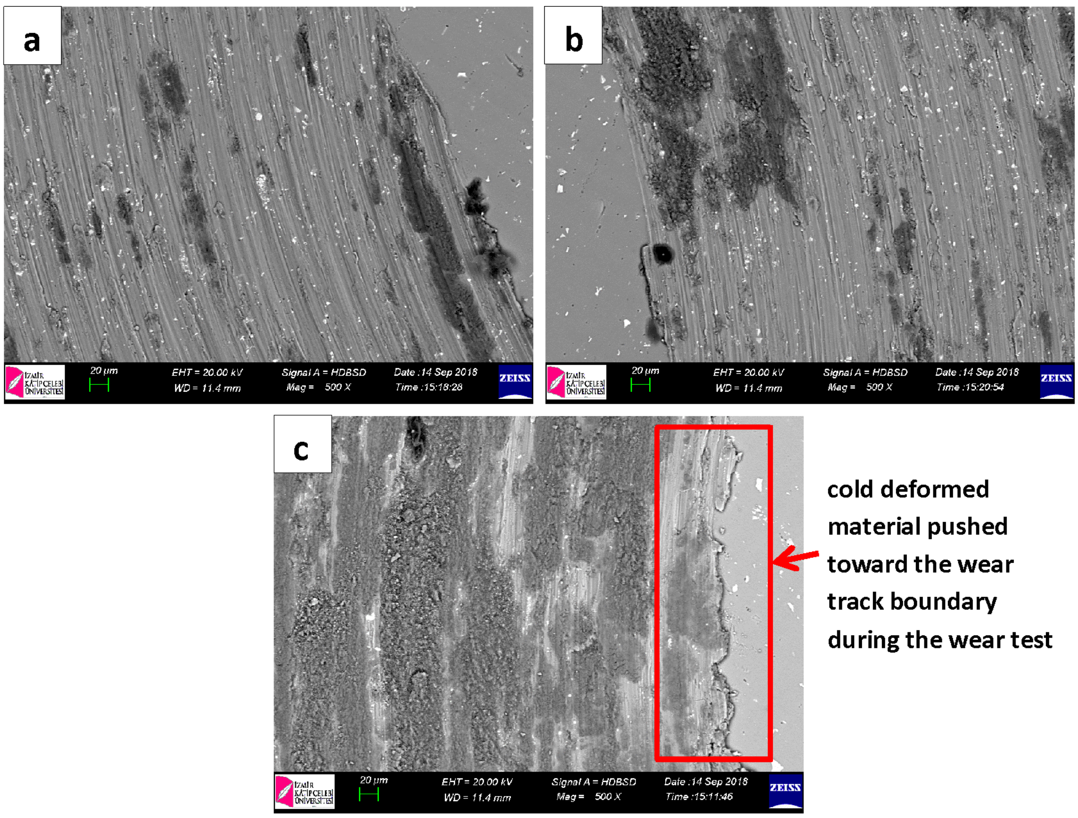

Figure 12. Worn surfaces of aged AA2010 alloy for a) 16 h, b) 18 h, and c) 22 h.

that exhibits peak hardness. In further stages of the wear test, overaged sample showed minimum wear loss. This finding is associated with the strain hardening ability of the material. After the wear test, the effect of cold deformation was revealed by micro hardness test. The overaged sample with the minimum hardness value exhibited the maximum hardness on the worn surface after the wear test. This, can be explained by the cold deformation ability of overaged sample. Due to its relatively low hardness, overaged sample can be deformed easier under the cyclic load of wear test. Consequently, cold deformation of the overaged sample provides better wear resistance, unexpectedly. Lindroos *et al.* (2015) stated that, the wear rate can decrease due to the significant surface work hardening during the repeated loading of the wear test. Similarly, De Mello *et al.* (2017) asserted that higher level of strain increases the internal energy of the material that promotes surface oxidation, and therefore, it decreases the wear rate. Because, the surface oxidation reduces the friction between the metal surface and the counterpart, if the wear test is carried out in air media without a lubricant (Buckley, 1981). Friction coefficient values measured during the wear test support the formation of surface oxidation in overaged sample more than the others. The average values of friction coefficient (μ) were obtained 0.68, 0.64, and 0.49 for 16 h., 18 h., and 22 h. aged samples, respectively. Owing to the reduced hardness of overaged sample, counterpart easily deformed surface and increased the concentration of dislocations. Strained metal with a high level of dislocation concentration is chemically more active on the surface (Buckley, 1981), hence it is prone to oxidation during the wear test and reduce the friction coefficient as observed in overaged sample. SEM-EDX analysis of wear debris of 22 h aged specimen consists of aluminum and oxygen. It proves the existence of oxidation of aluminum (Fig. 11). Al_2O_3 on worn surface not only arises from the oxidation of metal surface, but also the detached particles of alumina ball as a counterpart.

Continuous scratches were observed on the worn surface of 16 and 18 h aged specimens. Wear track shows a sharp boundary between the aluminum matrix and worn surface of specimens aged for 16 and 18 h. On the contrary, the overaged sample exhibits the remains of cold deformed material along the wear track boundary (Fig. 12).

4. CONCLUSIONS

AA2010 alloy which is suitable for vehicle body construction was exposed to artificial aging. The effect of aging time on corrosion, hardness and wear resistance was discussed in this study. The findings can be summarized as follows:

- Microstructure of aged AA2010 alloy consists of Al-Fe intermetallic particles in addition to Mg_2Si, $MgZn_2$, Al_2Cu and Al_2CuMg precipitates in aluminum matrix.

- The minimum corrosion rate was obtained by reaching the peak strength aging time that is found to be 18 h for the given alloy. Overaging reduced the corrosion resistance due to the anodic phases which tend to precipitate along the grain boundary. Both the intergranular and pitting corrosion mechanisms were observed in the aged AA2010 alloy. However, intergranular corrosion became more significant for the overaged sample.

- Peak hardness of 120 HV2 was achieved by applying 18 h artificial aging. AA2010 alloy became overaged at 22 h and the hardness decreased to 111 HV2. The overaged sample showed superior wear resistance, although it has the lowest hardness value. Micro hardness measurements taken from the wear track revealed that decreased hardness of the overaged sample provided more cold deformation resulted in strain hardening and oxidation that influence the wear resistance positively together.

REFERENCES

Abarghouie, S.M.R.M., Reihani, S.M.S. (2010). Investigation of friction and wear behaviors of 2024 Al and 2024 Al/SiCp composite at elevated temperatures. *J. Alloys Compd.* 501 (2), 326-332. https://doi.org/10.1016/j.jallcom.2010.04.097.

Andreatta, F., Terryn, H., De Wit, J.H.W. (2004). Corrosion behaviour of different tempers of AA7075 aluminium alloy. *Electrochim. Acta*. 49 (17-18), 2851-2862. https://doi.org/10.1016/j.electacta.2004.01.046.

Arunachalam, S.R., Dorman, S.E.G., Buckley, R.T., Conrad, N.A., Fawaz, S.A. (2018). Effect of electrical discharge machining on corrosion and corrosion fatigue behavior of aluminum alloys. *Int. J. Fatigue* 111, 44-53. https://doi.org/10.1016/j.ijfatigue.2018.02.005.

Baker, H. (1992). *ASM Handbook Volume 3*: *Alloy Phase Diagrams*. ASM International.

Bilgiç, S. (2018). *Galvanic Corrosion. The Eurasia Proceedings of Science, Technology, Engineering and Mathematics.* SRES Publishing, pp. 259-262.

Buckley, D.H. (1981). *Tribology Series*. Elsevier.

Burt, V. (2015). *Corrosion in the Petrochemical Industry*. ASM International.

Çavdar, U., Taştan, M., Gökozan, H., Soy, G., Sarı Çavdar, P. (2021). Heat Treatment of 2024 and 5083 Aluminum Materials by Induction, a Competitive Method, and Cost Analysis. *J. Inorg. Organomet. Polym.* 31, 1754–1763. https://doi.org/10.1007/s10904-020-01813-1.

Chen, G.S., Gao, M., Wei, R.P. (1996). Microconstituent-induced pitting corrosion in aluminum alloy 2024-T3. *Corrosion* 52 (1), 8-15. https://doi.org/10.5006/1.3292099.

De Mello, J.D.B., Labiapari, W.S., Ardila, M.A.N., Oliveira, S.A.G., Costa, H.L. (2017). Strain hardening: can it affect abrasion resistance?. *Tribol. Lett*. 65 (2), 67. https://doi.org/10.1007/s11249-017-0850-8.

Gharavi, F., Matori, K.A., Yunus, R., Othman, N.K., Fadaeifard, F. (2015). Corrosion behavior of Al6061 alloy weldment produced by friction stir welding process. *J. Mater. Res. Technol*. 4 (3), 314-322. https://doi.org/10.1016/j.jmrt.2015.01.007.

Hussey, B., Wilson, J. (1998). *Light Alloys: Directory and Databook*. Chapman & Hall.

Kaçar, H., Atik, E., Meriç, C. (2003). The effect of precipitation-hardening conditions on wear behaviours at 2024 aluminium wrought alloy. *J. Mater. Process. Tech.* 142 (3), 762-766. https://doi.org/10.1016/S0924-0136(03)00642-3.

Kaczmar, J.W., Naplocha, K. (2010). Wear behaviour of composite materials based on 2024 Al-alloy reinforced with δ alumina fibres. *J. Achiev. Mater. Manuf. Eng.* 43 (1), 88-93.

Kang, J., Fu, R.D., Luan, G.H., Dong, C.L., He, M. (2010). In-situ investigation on the pitting corrosion behavior of friction stir welded joint of AA2024-T3 aluminium alloy. *Corros. Sci.* 52 (2), 620-626. https://doi.org/10.1016/j.corsci.2009.10.027.

Krishna, K.G., Das, G., Venkateswarlu, K., Kumar, K.H. (2017). Studies on Aging and Corrosion Properties of Cryorolled Al–Zn–Mg–Cu (AA7075) Alloy. *Trans. Indian Inst. Met*. 70 (3), 817-825. https://doi.org/10.1007/s12666-017-1064-3.

Liao, C.M., Olive, J.M., Gao, M., Wei, R.P. (1998). In-situ monitoring of pitting corrosion in aluminum alloy 2024. *Corrosion* 54 (6), 451-458. https://doi.org/10.5006/1.3284873.

Lindroos, M., Valtonen, K., Kemppainen, A., Laukkanen, A., Holmberg, K., Kuokkala, V.T. (2015). Wear behavior and work hardening of high strength steels in high stress abrasion. *Wear* 322-323, 32-40. https://doi.org/10.1016/j.wear.2014.10.018.

Liu, Y., Mol, J.M.C., Janssen, G.C.A.M. (2016). Combined Corrosion and Wear of Aluminium Alloy 7075-T6. *J. Bio. Tribo. Corros*. 2 (2), 2-9. https://doi.org/10.1007/s40735-016-0042-3.

Menan, F., Henaff, G. (2009). Influence of frequency and exposure to a saline solution on the corrosion fatigue crack growth behavior of the aluminum alloy 2024. *Int. J. Fatigue.* 31 (11-12), 1684-1695. https://doi.org/10.1016/j.ijfatigue.2009.02.033.

Meyveci, A., Karacan, İ., Durmuş, H., Çaligülü, U. (2009). Using of Artificial Neural Networks For Modelling Wear Behaviour Of Aged 2024 and 6063 Aluminium Alloy. *Journal of Yaşar University* 4 (13), 2062-2077. https://dergipark.org.tr/tr/download/article-file/179224.

Meyveci, A., Karacan, İ., Çaligülü, U., Durmuş, H. (2010). Pin-on-disc characterization of 2xxx and 6xxx aluminium alloys aged by precipitation age hardening. *J. Alloys Compd*. 491 (1-2), 278-283. https://doi.org/10.1016/j.jallcom.2009.10.142.

Meyveci, A., Karacan, İ., Fırat, E.H., Çaligülü, U., Durmuş, H. (2011). Study of wear of aged aluminum alloys 2XXX and 6XXX within the manova statistical analysis. *Met. Sci. Heat. Treat.* 53 (3), 173-175. https://doi.org/10.1007/s11041-011-9363-5.

Meyveci, A., Karacan, İ., Durmuş, H., Çaligülü, U. (2012). Artificial Neural Network (ANN) Approach to Hardness Prediction of Aged Aluminium 2024 and 6063 Alloys. *Mater. Test.* 54 (1), 36-40. https://doi.org/10.3139/120.110290.

Mishra, A.K., Balasubramaniam, R. (2007). Corrosion inhibition of aluminum alloy AA 2014 by rare earth chlorides. *Corros. Sci.* 49 (3), 1027-1044. https://doi.org/10.1016/j.corsci.2006.06.026.

Sadeler, R., Totik, Y., Gavgali, M., Kaymaz, I. (2004). Improvements of fatigue behaviour in 2014 Al alloy by solution heat treating and age-hardening. *Mater. Design* 25 (5), 439-445. https://doi.org/10.1016/j.matdes.2003.12.003.

Staley, J.T. (2016). Corrosion of Aluminium Aerospace Alloys. *Mater. Sci. Forum* 877, 485-491. https://doi.org/10.4028/www.scientific.net/MSF.877.485.

Sun, H.T., Wang, J., Shen, G.Z., Hu, P. (2013). Application of warm forming aluminum alloy parts for automotive body based on impact. *Int. J. Automot. Technol.* 14 (4), 605-610. https://doi.org/10.1007/s12239-013-0065-4.

Tariq, F., Naz, N., Baloch, R.A. (2012). Characterization of material properties of 2xxx series al-alloys by non destructive testing techniques. *J. Nondestruct. Eval.* 31 (1), 17-33. https://doi.org/10.1007/s10921-011-0117-5.

Taştan, M., Gökozan, H., Sarı Çavdar, P., Soy, G., Çavdar, U. (2019). Analysis of artificial aging with induction and energy costs of 6082 Al and 7075 Al materials. *Rev. Metal.* 55 (1), e137. https://doi.org/10.3989/revmetalm.137.

Totten, G.E., Tiryakioglu, M., Kessler, O. (2018). *Encyclopedia of Aluminum and Its Alloys*. CRC Press.

Vieira, A.C., Pinto, A.M., Rocha, L.A., Mischler, S. (2011). Effect of Al_2Cu precipitates size and mass transport on the polarisation behaviour of age-hardened Al–Si–Cu–Mg alloys in 0.05 M NaCl. *Electrochim. Acta* 56 (11), 3821-3828. https://doi.org/10.1016/j.electacta.2011.02.044.

Wang, S.C., Starink, M.J. (2005). Precipitates and intermetallic phases in precipitation hardening Al–Cu–Mg–(Li) based alloys. *Int. Mater. Rev.* 50 (4), 193-215. https://doi.org/10.1179/174328005X14357.

Yasakau, K.A., Zheludkevich, M.L., Lamaka, S.V., Ferreira, M.G.S. (2007). Role of intermetallic phases in localized corrosion of AA5083. *Electrochim. Acta* 52 (27), 7651-7659. https://doi.org/10.1016/j.electacta.2006.12.072.